eCELLS & MATERIALS

OPEN ACCESS

DEVELOPMENT OF A 3D-PRINTED BIOABSORBABLE COMPOSITE SCAFFOLD WITH MECHANICAL PROPERTIES SUITABLE FOR TREATING LARGE, LOAD-BEARING ARTICULAR CARTILAGE DEFECTS

M. Joyce[1,2,3], T. Hodgkinson[1], M. Lemoine[1,2,3], A. González-Vázquez[1,2,3], D.J. Kelly[1,2,3] and F.J. O'Brien[1,2,3,*]

[1] Tissue Engineering Research Group (TERG), Department of Anatomy and Regenerative Medicine, Royal College of Surgeons in Ireland (RCSI), Dublin, Ireland
[2] Trinity Centre for Biomedical Engineering (TCBE), Trinity College Dublin, Dublin, Ireland
[3] Advanced Materials and BioEngineering Research (AMBER) Centre, Dublin, Ireland

Abstract

Extracellular matrix (ECM) biomaterials have shown promise for treating small artucular-joint defetcs. However, ECM-based biomaterials generally lack appropriate mechanical properties to support physiological loads and are prone to delamination in larger cartilage defects. To overcome these common mechanical limitations, a collagen hyaluronic-acid (CHyA) matrix, with proven regenerative potential, was reinforced with a bioabsorbable 3D-printed framework to support physiological loads. Polycaprolactone (PCL) was 3D-printed in two configurations, rectilinear and gyroid designs, that were extensively mechanically characterised. Both scaffold designs increased the compressive modulus of the CHyA matrices by three orders of magnitude, mimicking the physiological range (0.5-2.0 MPa) of healthy cartilage. The gyroid scaffold proved to be more flexible compared to the rectilinear scaffold, thus better contouring to the curvature of a femoral condyle. Additionally, PCL reinforcement of the CHyA matrix increased the tensile modulus and allowed for suture fixation of the scaffold to the subchondral bone, thus addressing the major challenge of biomaterial fixation to articular joint surfaces in shallow defects. *In vitro* evaluation confirmed successful infiltration of human mesenchymal stromal cells (MSCs) within the PCL-CHyA scaffolds, which resulted in increased production of sulphated glycosaminoglycans (sGAG/DNA; $p = 0.0308$) compared to non-reinforced CHyA matrices. Histological staining using alcian blue confirmed these results, while also indicating greater spatial distribution of sGAG throughout the PCL-CHyA scaffold. These findings have a great clinical importance as they provide evidence that reinforced PCL-CHyA scaffolds, with their increased chondroinductive potential and compatibility with joint fixation techniques, could be used to repair large-area chondral defects that currently lack effective treatment options.

Keywords: Bioregenerative, pro-chondrogenic, 3D-printed scaffolds, cartilage repair, mechano-transduction, biomaterial fixation.

***Address for correspondence**: F.J. O'Brien, Royal College of Surgeons in Ireland, Dublin, Ireland
Email: FJObrien@RCSI.com

List of Abbreviations

ANOVA	analysis of variance
CAD	computer-aided design
CCM	complete chondrogenic medium
CHyA	collagen and hyaluronic acid matrices
CI	confidence interval
COL2	collagen type II
DAB	3,3'-diaminobenzidine
DMEM	Dulbecco's modified eagle medium
DPX	dibutyl phthalate xylene
EDAC	1-ethyl-3-(3(dimethlaminopropyl)-carbodimide
ECM	extracellular matrix
FBS	foetal bovine serum
FDA	Food and Drug Administration
FDM	fused deposition modelling
HyA	hyaluronic acid
HRP	horseradish peroxidase
IHC	immunohistochemical
IHC-BB	IHC blocking buffer
IPN	interpenetrating hydrogel
MEW	melt-electrospinning writing
MSC	mesenchymal stromal cell
NHS	N-hydroxysuccinimide
NIH	National Institutes of Health
PBS	phosphate-buffered saline

PCL	polycaprolactone
ROCK	Rho kinase
SEM	scanning electron Microscopy
sGAG	sulphated glycosaminoglycans
STL	standard tessellation language
TGFβ-3	transforming growth factor beta 3

Introduction

Articular cartilage is an avascular, slightly porous, viscoelastic connective tissue found in synovial joints covering the end of long bones (Camarero-Espinosa *et al.*, 2016). In addition to providing a smooth, low-friction surface for movement, articular cartilage acts as a shock absorber to distribute physiological loads evenly across the surface of the subchondral bone (Di Luca *et al.*, 2015). Cartilage's hydrophilic ECM is comprised of proteoglycans and sGAG, which are critical to the form and function of the tissue (Alford *et al.*, 2005). Once cartilage is damaged, chondrocytes, as a result of their low cell density and limited mobility through the dense matrix, are unable to repair the damaged ECM, which ultimately leads to a structural and functional failure of the hyaline tissue. With no effective clinical interventive repair options currently available, the condition of the damaged cartilage often progressively worsens over time leading to osteoarthritis (Hodgkinson *et al.*, 2022a; 2022b).

Tissue engineering approaches work to overcome the limited reparative capacity of mature cartilage by combining appropriate biomaterials, biochemical cues and cells to facilitate the formation of *de novo* cartilage to replace damaged tissue. Clinical success of these approaches has been limited, motivating the development of more advanced biomaterial scaffolds capable of supporting functional cartilage regeneration. The porous freeze-dried composite CHyA developed by the authors has been shown to accurately recapitulate the native cartilage ECM (Haugh *et al.*, 2009; Intini *et al.*, 2022a; Matsiko *et al.*, 2012, 2015). These CHyA matrices have also been utilised as the chondral layer in a multi-layered osteochondral matrix that, when combined with a microfracture surgical technique, has been shown to support the differentiation of bone-marrow-derived MSCs into chondrocytes in large-animal *in vivo* studies (Levingstone *et al.*, 2016, 2021, 2022; Stack *et al.*, 2017). Then, the chondrocytes are capable of synthesising *de novo* cartilage ECM components, including COL2, aggrecan, hyaluronan and sGAGs (Matsiko *et al.*, 2012, 2015; Unterman *et al.*, 2012). While promising, the use of these matrices, along with comparable hydrogel biomaterials, has been confined *in vivo* to focal osteochondral defects. For the treatment of larger defects, further improvements are required, such as reinforcement to match the compressive modulus of the healthy articular cartilage (0.5-2.0 MPa) to support physiological loads (Haugh *et al.*, 2011; Kabir *et al.*, 2021).

The first aim of the present study was to mechanically reinforce the favourable microporous architecture and biological functionality of a CHyA matrix with a 3D-printed bioabsorbable scaffold so it would be strong enough to withstand load-bearing forces. Maintaining the favourable porous structure under physiological loads is essential to support proper cellular infiltration (Matsiko *et al.*, 2014). Unlike focal chondral defects, large-area chondral defects experience greater lateral frictional forces, increasing the risk of delamination of pro-chondrogenic biomaterials from chondral defects (Lotz *et al.*, 2021). Therefore, proper biomaterial fixation within a large-area chondral defect is essential to prevent delamination and promote adequate cellular infiltration for successful tissue integration (Nehrer *et al.*, 1998). In addition to increasing the compressive modulus, a secondary aim of this study was to utilise the developed bioabsorbable reinforcing scaffold structure as a secure site for fixation to the subchondral bone using osteo-suture anchors. Historically, suture fixation has not paired well with mechanically weak biomaterials, as the suture tends to tear through soft biomaterials (DuRaine *et al.*, 2015; Hunziker *et al.*, 2008). An effective reinforcing structure for a natural ECM-based matrix, such as the CHyA scaffold, must also increase its tensile modulus to ensure it can be fixed effectively to the subchondral bone within a chondral defect. To accomplish this, PCL was selected as the biodegradable/bioabsorbable thermopolymer to create reinforced matrices due to its suitable mechanical properties, degradation profile, use in prior FDA-approved devices and compatibility with 3D printing (Chang *et al.*, 2018; Hutmacher *et al.*, 2001; MacCraith *et al.*, 2022; Moers-Carpi *et al.*, 2013; Zhang *et al.*, 2018). Utilising 3D printing to deposit PCL in the biofabrication process, with spatial precision, allows scaffold designs to undergo iterative progressions to better elucidate how design criteria affect mechanical properties, allowing specific optimisation for the repair of large-area chondral defects.

The microporous architecture of the CHyA scaffolds have been characterised extensively in the past, but it was unclear how the presence of PCL would influence or alter the microporous architecture when creating a composite PCL-ChyA scaffold (Intini *et al.*, 2022a; 2022b; Matsiko *et al.*, 2014). The main concern was that PCL could act as a thermal insulator, altering the ice crystal formation kinetics that govern the micropore formation in the freeze-drying process (Matsiko *et al.*, 2014). Furthermore, the hydrophobic properties of PCL might repel the more polar aqueous ChyA from fully infiltrating into the PCL scaffold structure, creating large void spaces. Therefore, PCL-CHyA composite scaffolds were characterised to determine if PCL interfered with the biofabrication process to alter the favourable microporous architecture of CHyA matrices.

The objective of the present study was to design, fabricate and investigate the effects of mechanically

reinforcing CHyA matrices with different biodegradable scaffold designs for their putative use in the treatment of large load-bearing articular cartilage defects. Bio-fabricated reinforced PCL-CHyA scaffolds were assessed against many design criteria which fell under the umbrella of 3 overarching criteria: to i) increase the compressive modulus of the ECM-based material; ii) be compatible with secure fixation in large articular cartilage defects; iii) permit cellular infiltration and chondrogenic differentiation. Successfully meeting these 3 overarching design criteria could eventually offer a bioregenerative mechanically reinforced scaffold that could be used as an off-the-shelf solution to repair large-area chondral defects.

Materials and Methods

Design and fabrication of 3D-printed PCL reinforcing scaffolds

STL files for 3D printing were created using Onshape (Onshape, Boston, MA, USA) CAD software before being imported into Repetier Host with open source Ultimaker Cura software (V 2.1.2) to slice the file and create a G-code that could be interpreted by the 3D printer. Initially, many different design features were selected for, or against, regardless of the shape of the part. For example, perimeter boundary toolpaths were excluded, as they would cause a size/shape-dependent response on the mechanical properties, while also likely inhibiting perpendicular cellular infiltration into the scaffold (Liu *et al*., 2020). To aid in this design process, the study had specific application criteria (outlined below). These were established and prioritised in order of importance to help weigh, at times, competing data from different evaluation techniques.

Application specific toolpath infill design criteria

The following design criteria were applied in the development of the 3D-printed framework.

- Increase compressive modulus of CHyA matrix to 2.0 > MPa > 0.5 (Kabir *et al*., 2021; Liu *et al*., 2020; Nieminen *et al*., 2004).
- Allow homogenous CHyA matrix incorporation, with microarchitecture similar to non-reinforced CHyA.
- Not inhibit cellular migration into CHyA or inhibit chondrogenesis.
- Be flexible to fit the contour of a femoral/tibial condyle.
- Be compatible with fixation techniques to the subchondral bone.
- Be scalable to proceed from mechanical testing to *in vitro* and to large-animal *in vivo* models.
- Be reproducible with minimal variation.
- Contain as little PCL as possible as biodegradation over time might produce a void space prone to abscess or induce an immune response.
- Reduce production time, when reasonable.

There are many infill toolpath designs available, although some are more conducive to some applications over others (Gupta *et al*., 2020; Heras Murcia *et al*., 2020). Different scaffold infill designs available through the Ultimaker Cura software were selected and 3D-printed so they could be evaluated under the aforementioned criteria. The two most important of which, from a mechanical perspective, were to increase the compressive modulus to support load-bearing forces, while also producing a scaffold that was flexible enough to contour the curvature of an articular joint with minimal force. These two design criteria often have a direct opposing relationship with the material volume required. For example, more material would typically increase the compressive modulus but make the scaffold less flexible. Then, scaffold designs were holistically evaluated across numerous design criteria for selection. While many different scaffold designs were initially investigated, after printing prototype versions, many designs were disqualified prior to undergoing rigorous mechanical testing regiments. Ultimately, two scaffold designs were brought forward for extensive mechanical characterisation following an initial screening process. The two scaffolds (rectilinear, gyroid) were both continuous, non-intersecting toolpaths with a 90° offset between layers. Other open-source non-continuous or intersecting toolpath designs, represented by the star or triangle infill pattern, were also printed for initial screening.

To fabricate the scaffolds, PCL (Polysciences, Germany) was printed using an Allevi II bioprinter (Allevi, Philadelphia, PA, USA) at 100 °C using a metal 27-gauge luer lock needle (Fisnar, Eden Prairie, MN, USA) at 6.2×10^5 Pa to produce the various scaffold designs. PCL is non-polar and moderately hydrophobic, which can inhibit aqueous matrix infiltration. To overcome this, printed PCL structures were soaked in 3 mol/L NaOH for 48 h. NaOH cleaves ester bonds in the PCL to expose more polar groups, increasing its hydrophilicity (Estes *et al*., 2021; Green *et al*., 2018). NaOH has also been shown to roughen, on a microscopic scale, the otherwise smooth surface of extruded PCL (Gupta *et al*., 2019).

Incorporation of CHyA matrix into 3D-printed scaffolds

CHyA slurry was created by blending 0.9 g of bovine collagen type I (Collagen Matrix, Paramus, NJ, USA) (0.25 % w/v) and 0.9 g of collagen type II (Symatese, Chaponost, France) (0.25 % w/v) in 300 mL of 0.5 mol/L acetic acid. 0.18 g of hyaluronic acid (1.50-1.80 MDa) (Contipro,Dolní Dobrouč, Czech Republic) (0.05 % w/v) was added dropwise while the slurry continued to blend, as previously described by Matsiko *et al.* (2012). Then, CHyA was degassed before being combined with 3D-printed PCL scaffolds. Next, PCL-CHyA was freeze-dried for 48 h using previously described techniques (Matsiko *et al.*, 2014). After freeze-drying was complete, PCL-CHyA scaffolds were crosslinked for 2 h at pH 5.0 using

EDAC (Sigma-Aldrich) and NHS (Sigma-Aldrich) in a 5:2 molar ratio (EDAC:NHS) using 70 % ethanol as a solvent. Finally, scaffolds were rinsed three times with sterile PBS prior to use.

Mechanical characterisation of PCL-CHyA scaffolds

PCL-CHyA scaffolds underwent mechanical characterisation to assess their feasibility to be used in human articular joints. Scaffolds underwent cyclical (5 cycles) uniaxial compressive strain up to 20 % using a Zwick/Roell Z005 (Zwick/Roell Inc, Germany) with a 50 N load cell at a rate 0.15 mm/s. The compressive modulus of the different PCL scaffold designs was determined from stress *vs.* strain curve data (Gupta *et al.*, 2019). A 3-point bend test was performed on [30 × 30 × (1.7-2.25) mm] PCL-CHyA scaffolds to determine how much force was required to bend scaffolds to fit the contour of a human tibial or femoral condyle. A 50 N load cell between two rollers 12 mm apart was used to deflect scaffolds 2 mm past neutral at a rate of 0.15 mm/s to determine the maximum force required to bend different scaffold designs. Different PCL scaffold designs influenced mechanical behaviour, producing some parts that behaved more or less anisotropically than others. Therefore, "square" (3 × 3 cm) PCL scaffolds were bent along the X axis, rotated 90° and bent perpendicular to the previous orientation to determine the greatest force required to bend anisotropic behaving PCL-CHyA scaffolds.

Assessment of PCL-CHyA scaffold fixation to subchondral bone

Three different osteo-suture anchors were investigated to determine their effectiveness in securing PCL-CHyA scaffolds within a chondral defect. The first was a commercially available osteo-suture screw (Smith&Nephew Twinfix Ti, Andover, MA, USA) (Fig. 1**a**). However, as metal suture anchors might prevent tissue regeneration in the volume they occupied, bioabsorbable press-fit cylindrical osteo-anchors were also fabricated with PCL using an Allevi 3D printer. The cylindrical anchors were 4 or 6 mm in diameter with a height of 6.5 mm (Fig. 1 **b**,**c**). Suture thread was looped vertically through the core of the cylinder so that the superficial circular face could be affixed using a suture to a load cell for mechanical testing or through PCL-CHyA scaffold for fixation. The 3 osteo-suture anchors were implanted into a cadaveric porcine tibial condyle (Fig. 1**d**) (FX Buckley, Dublin, Ireland) and attached using Mersilk suture thread (Ethicon, Somerville, NJ, USA) to a 50 N load cell, while uniaxial tensile force was applied until anchor failure was observed. By analysing how much force was required to bend the scaffold designs to the curved contour of a condyle, it was possible to determine whether the anchor was strong enough to hold the PCL scaffold securely to the subchondral bone. To determine how much tensile force a PCL-CHyA scaffold could withstand, suture thread was looped around 1 column of PCL struts in the PCL-CHyA scaffold or looped around 3 columns of PCL struts (Fig. 1**e**). Then, the scaffold was immobilised as uniaxial tensile force was applied until scaffold failure. Non-reinforced CHyA were also tested in a similar fashion, without the PCL to anchor the suture thread.

Cell culture and seeding of hMSCs on PCL-CHyA scaffolds

Bone-marrow-derived human MSCs (P5, Lonza) were isolated and characterised as previously described (Barreto *et al.*, 2017) before being seeded on sterile cylindrical scaffolds (10 × 2 mm) at a density of 5×10^5 cells/scaffold. Half the cells (2.5×10^5) were seeded on the PCL-CHyA scaffolds or CHyA matrices and allowed to attach for 30 min before the scaffold/matrix were flipped and the opposite side was seeded with the remaining 2.5×10^5 MSCs. These were allowed to attach for an additional 30 min before filling each well with 2 mL of growth medium for 24 h. Growth medium for cellular expansion consisted of low-glucose DMEM with L-glutamine (Sigma-Aldrich) and supplemented with 10 % (v/v) FBS (ThermoFischer), 1 % (v/v) penicillin/streptomycin (ThermoFischer) and 0.2 % (v/v) primocin (Invivogen). After 24 h, growth medium

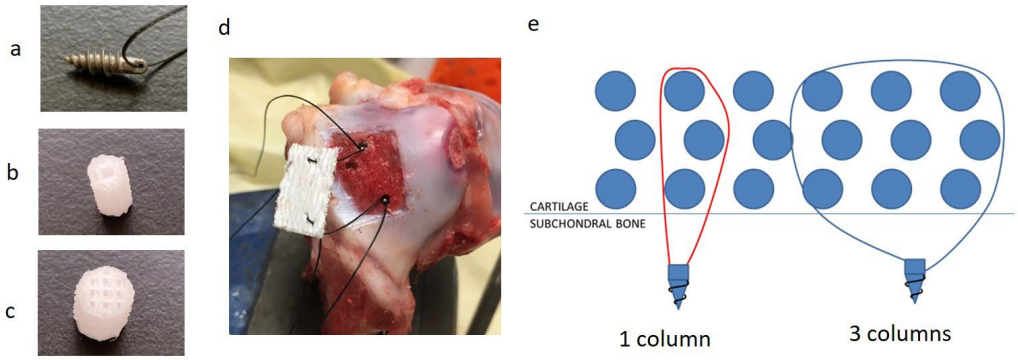

Fig. 1. Form and function of subchondral fixation anchors. (**a**) Twinfix-Ti 2.8 osteochondral suture anchor, 4 and 6 mm diameter (**b**,**c** respectively) 3D-printed osteochondral anchors for fixation testing. (**d**) Demonstration of how a reinforced PCL-CHyA (2 × 1 × 0.2 cm) could be fixed with sutures to a recessed subchondral anchor. (**e**) A cross-sectional schematic depicting how the suture tensile load was distributed across 1 or 3 PCL columns.

was replaced with CCM. Then, cells-seeded scaffolds were incubated up to 28 d at 37 °C with 5 % CO_2. Medium changes were performed every 3 d. CCM consisted of high-glucose DMEM (Sigma-Aldrich) supplemented with dexamethasone (100 nmol/L, Sigma Aldrich), ascorbic acid (50 μg/mL, Sigma-Aldrich), L-proline (40 μg/mL, Sigma-Aldrich), ITS+ supplement (1×, BD Biosciences, Wokingham, UK), sodium pyruvate (0.11 mg/mL, Sigma-Aldrich), penicillin/streptomycin (1 %, ThermoFischer), primocin (0.2 %, Invivogen) and TGFβ-3 (10 ng/mL, Peprotech).

Biochemical characterisation of cell-seeded PCL-CHyA scaffolds

sGAG and DNA quantification were both performed by first lysing cell-seeded PCL-CHyA and CHyA using consecutive freeze-thaw cycles at − 80 °C prior to papain (0.01% wt/wt) digestion (Sigma-Aldrich) overnight at 65 °C. Following incubation, the respective assay manufacturer's protocols were followed for the Blyscan sGAG assay (Biocolor, Carrickfergus, UK) (Matsiko *et al*., 2015) and the Quant-iT PicoGreen dsDNA assay (Invitrogen). In brief, sGAG were quantified by binding with Blyscan dye and absorbance measured at a wavelength of 656 nm. sGAG concentration was determined by comparison to a standard curve. Similarly, DNA was quantified by intercalating dsDNA with Picogreen and measuring the fluorescence at a wavelength of 538 nm. Then, dsDNA concentration was determined by comparison to a standard curve.

Histological evaluation of PCL-CHyA scaffolds

Histological analysis was carried out in two ways. Prior to seeding scaffolds with cells, samples were embedded in JB-4 (Polysciences Inc, Hirschberg an der Bergstrasse, Germany), which offers higher morphological resolution compared with paraffin-wax embedding. These samples were used for pore-size analysis to characterise what effect PCL may have on the micropore formation. Embedding was carried out following the manufacturer's protocol. Then, samples were sliced into 10 μm-thick sections using a Leica RM2255 microtome, stained with toluidine blue to better visualise microporous architecture and imaged using a Nikon Eclipse 90i microscope and a Nikon DS RiL camera. Multiple images were imported into a pore topology analysing script (Sigmedia Research Group, Department of Electrical Engineering, TCD, Dublin, Ireland) in MatLab R2019a (Mathworks Inc) as previously described (Matsiko *et al*., 2014). The software defined the image in binary threshold values that were used for measurement of CHyA pore diameter in an automated process to accurately measure multiple pores per image. Next, the mean pore size from multiple images was calculated using 20 images from PCL-reinforced or non-reinforced CHyA.

For histological analysis, scaffolds that had been seeded with cells were fixed in 10 % formalin and dehydrated in an ethanol gradient before being soaked in xylene, which also removed the PCL structure. Then, samples were embedded in paraffin-wax before being sliced into 10 μm-thick sections and imaged using the same Leica and Nikon equipment as for JB-4. Finally, sections were stained with pH 1 alcian blue, which selectively binds sGAG (Layton *et al*., 2019). Nuclear fast red was used as a counterstain. ImageJ software (NIH) was used to add scale bars to images.

IHC analyses were performed on histological sections to characterise the ECM deposition spatially. Samples were dewaxed as before and treated with pronase [0.0125 % (wt/wt), Merk] and hyaluronidase [1% (wt/wt), Sigma-Aldrich] for antigen retrieval. Sections were exposed to H_2O_2 (20 min) to reduce endogenous enzyme activity prior to incubation with IHC-BB for 30 min at room temperature. IHC-BB contained 1 % BSA and 0.5 % goat serum (ab7481, Abcam) in PBS. Sections were rinsed in PBS and incubated overnight at 4 °C with a mouse primary antibody for COL2 (SC52658, Santa Cruz) at a 1:100 dilution in 1 % IHC-BB. Sections were rinsed with PBS before incubation with goat anti-mouse IgG antibodies conjugated with HRP (ab6728, Abcam) in a 1:500 dilution for 1 h at room temperature. Samples were treated with avidin peroxidase, following the manufacturer's protocol (PK-6101, Vector Laboratories, USA), in blocking buffer (45 min) and rinsed with PBS. Then, they were treated with a DAB substrate peroxidase kit (SK-4100, Vector Laboratories, USA) for 12 min. Next, sections were rinsed with PBS, 100 % ethanol and xylene, before being mounted using DPX (Sigma-Aldrich) and coverslips. Finally, sections were imaged using a Nikon DS RiL camera.

Statistics

Statistical analysis was performed using Prism GraphPad software (Prism) using a one-way ANOVA with a Tukey *post-hoc* test for multiple comparisons set a 95 % CI, except for Fig. 5**c** where a Fisher LSD test was utilised. Data are presented as mean value ± standard deviation, unless noted otherwise. Two-tailed *t*-tests were utilised with a 95 % CI when appropriate. Different colour data-points within a graph represent samples from different donor populations. * $p < 0.05$, ** $p < 0.01$, *** $p < 0.001$ and **** $p < 0.0001$.

Results

Design and biofabrication of 3D-printed PCL scaffolds

Scaffold designs underwent an initial screening to assess their printability before undergoing extensive mechanical characterisation. The star and triangle toolpath designs exhibited numerous interlayer intersections, with many toolpath start and termination points, highlighted by red circles in Fig. 2**a**,**b**. These toolpaths produced non-homogenous build-up of material at those points as a by-product

of the FDM 3D printing process (Web ref. 1). For these reasons, the star and triangle designs were disqualified from further characterisation. In contrast, the gyroid (Fig. 2**c**,**d**) and rectilinear (Fig. 2**e**,**f**) scaffolds were both continuous, non-intersecting toolpaths with a 90° offset between layers. Both the rectilinear and gyroid scaffold designs were brought forward for further mechanical testing.

Assessment of CHyA matrix infiltration and microporous architecture of resultant PCL-CHyA scaffolds

After CHyA and PCL scaffolds were combined during the freeze-drying biofabrication process, the composite PCL-CHyA scaffolds were assessed to ensure that PCL incorporation did not interfere with the formation of the microporous matrix architecture. Representative cross-sectional histological slices (n = 20) of PCL-CHyA and CHyA (Fig. 3**a**,**b**), respectively, were sampled to calculate the mean pore diameter. PCL reinforcement did not have a significant effect on the mean pore diameter (Fig. 3**c**), which was measured as 87.5 ± 7.51 μm and 90.6 ± 8.99 μm for the CHyA matrix and the PCL-CHyA scaffold, respectively. SEM cross-sectional imaging (Fig 3**d**) indicated good integration of the biomimetic CHyA matrix and PCL, with no large areas or voids in the microporous architecture being observed.

Mechanical characterisation of PCL-CHyA scaffolds

To determine their suitability for chondral repair, the compressive modulus of the gyroid and rectilinear PCL scaffolds were measured to assess if such reinforcement of the CHyA matrix would be sufficient for large-area load-bearing articular cartilage regeneration (0.5-2.0 MPa) (Kabir *et al.*, 2021). Both the gyroid and rectilinear scaffolds were able to accomplish this by raising the compressive modulus of CHyA matrices by three orders of magnitude from 0.6 KPa (± 0.0002) to 0.67 MPa (± 0.073) for the gyroid and to 0.65 MPa (± 0.132) for the rectilinear scaffold (Fig. 3**e**). When evaluated with a 3-point bend apparatus (Fig. 3**f**), using the lower and upper threshold of femoral condyle thickness (1.75 mm < cartilage thickness < 2.2 mm), the gyroid design showed no significant difference between the two heights tested, with the taller scaffold requiring slightly more force to bend it (2.67 ± 0.39 N). The thinner (1.75 mm) rectilinear scaffold required significantly more force to bend it (5.8 ± 0.44 N) compared to the gyroid design. Furthermore, the rectilinear scaffold presented a direct relationship with scaffold thickness and force required to bend it, with the taller 2.2 mm rectilinear scaffold requiring 9.6 ± 0.72 N to bend it, which was 3.6× more than the force required to bend the gyroid scaffold of the same dimensions to the same degree.

Scaffold fixation within chondral defects

To investigate the potential of the PCL-CHyA scaffolds to be securely held in a large-area hyaline cartilage defect, three subchondral anchors were tested to determine how much uniaxial tensile force they could withstand before dislodging from the subchondral bone. This was established by calculating the amount of force it took to bend the rectilinear

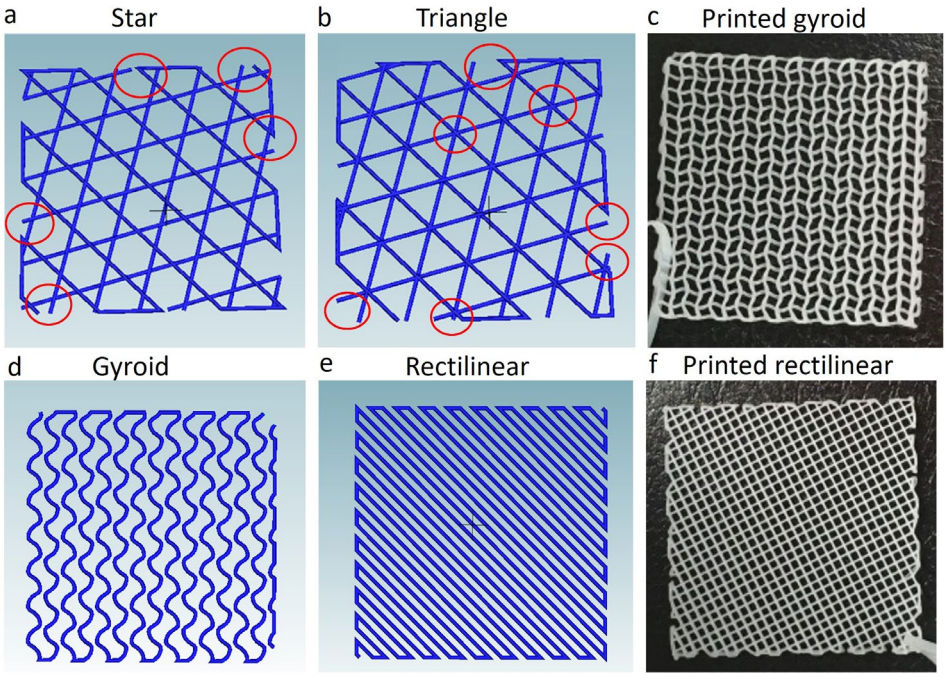

Fig. 2. Design and fabrication of PCL scaffolds for cartilage repair. (**a**,**b**,**d**,**e**) Representative images of single-layer toolpaths infill design (3 × 3 cm) (star, triangle, gyroid, rectilinear respectively), with (**a**,**b**) highlighting points of intersection and excessive toolpath start and stop points in red circles. (**c**,**f**) 3D-printed PCL scaffolds of the gyroid and rectilinear scaffold, respectively.

or gyroid scaffold to determine an appropriate pairing between subchondral anchors and scaffold design. The custom-developed cylindrical 4 mm and 6 mm diameter anchors required 3.3 ± 0.841 N and 10.06 ± 0.547 N of tensile force to dislodge them, respectively, while the Twinfix Ti anchors required more than 44.92 ± 0.016 N (Fig. 4**a**) (n = 3), although a greater force would begin to lift the steel vice grip that held the porcine tibia in place. All three mean values of uniaxial tensile force were significantly different from one another (p < 0.001). In order to determine how much tensile force the PCL scaffold could withstand prior to failure, suture thread was looped around 1 or 3 columns of PCL struts, as demonstrated in Fig. 1**e**. The PCL reinforcement significantly increased the uniaxial tensile force from 1.8 ± 1.42 N, with the CHyA matrix alone, to 11.63 ± 1.1 N, when anchored to 1 PCL column, or 22.57 ± 2.15 N, when the tensile force was distributed around 3 PCL columns (Fig. 4**b**) (n = 3).

Biological characterisation of PCL-reinforced CHyA indicated more sGAG deposition

Production of sGAG by cells in the scaffold was quantified to assess the potential of MSCs to undergo chondrogenic differentiation on the PCL-CHyA

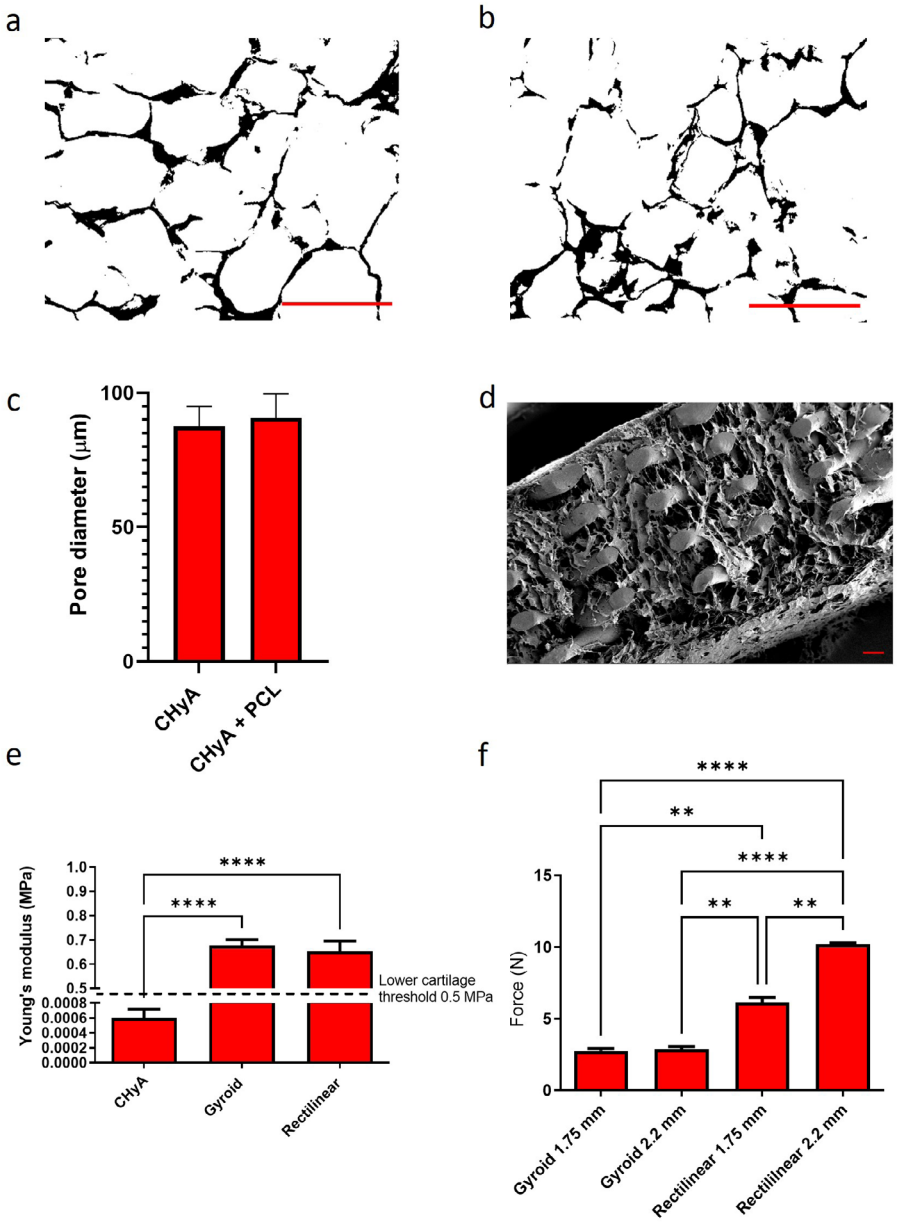

Fig. 3. Incorporation of PCL in CHyA improved mechanical properties without affecting CHyA microarchitecture. (**a**,**b**) Representative images of PCL reinforced and non-reinforced CHyA histological slices, respectively, (10 μm thickness) converted to binary images to measure and calculate mean pore size (scale bar = 200 μm). (**c**) Mean pore size of CHyA and PCL-CHyA (n = 20). (**d**) Cross-sectional SEM imaging of PCL-CHyA scaffold showed proper integration of CHyA matrix and PCL. Scale bar = 200 μm. (**e**) Young's compressive modulus of CHyA, gyroid and rectilinear scaffolds up to 20 % strain. Dashed line represents lower acceptable threshold for cartilage tissue (0.5 MPa) (n = 3) (**** p < 0.0001). (**f**) Force required to bend thin (1.75 mm) or thick (2.2 mm) gyroid and rectilinear scaffolds (n = 3) (** p < 0.01, **** p < 0.0001).

scaffolds. Total sGAG produced by human-derived MSCs on PCL-CHyA were significantly more (p = 0.0284) compared to non-reinforced CHyA after 28 d in culture (Fig. 5**a**). When total sGAG was normalised to DNA content within each sample (Fig. 5**b**), a similar trend was observed, with reinforced PCL-CHyA significantly increasing (p = 0.0204) sGAG/DNA over 28 d, while non-reinforced CHyA failed to show a significant increase in sGAG/DNA compared with its day 1 time point (p = 0.4592). To reduce variance from different donor cell populations, sGAG/DNA data were expressed as a relative fold change from the day 1 non-reinforced CHyA mean value for each donor population (Fig. 5**c**). Both the PCL-CHyA scaffold and CHyA matrix showed significantly increased relative production of sGAG/DNA (p = 0.0002 and p = 0.0411, respectively) over their day 1 levels. The PCL-CHyA scaffolds supported a significantly higher relative level of sGAG/DNA compared with non-reinforced CHyA after 28 d (p = 0.0308). Taken together, these results indicated that mechanical reinforcement of CHyA with PCL repeatedly increased the chondrogenic potential of CHyA matrices. This was a very encouraging result as the study aim was that the presence of the PCL framework would not inhibit sGAG production on the CHyA matrix. The fact that it instead enhanced it was an unexpected positive finding which warrants further investigation.

Histological analysis also confirmed more sGAG deposition on PCL-CHyA scaffolds compared to non-reinforced CHyA matrices. Alcian blue staining indicated more sGAG deposition on PCL-reinforced CHyA (10 × 2 mm) scaffolds at both superficial and

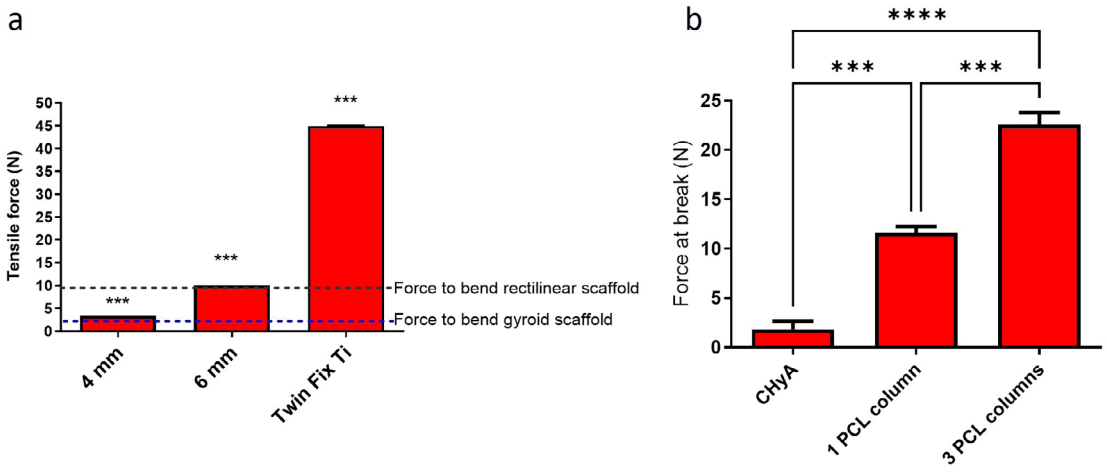

Fig. 4. PCL reinforcement of CHyA increased its capability to be held securely in an articular chondral defect. (**a**) Force (N) required to dislodge two 3D-printed cylindrical anchors (4 mm, 6 mm diameter) and a commercially available screw (Twinfix Ti) (n = 3). Blue and black dashed lines indicate force required to bend gyroid and rectilinear scaffolds respectively. (**b**) Tensile force (N) required to pull the suture thread out of the CHyA, PCL-CHyA around 1 PCL column and around 3 PCL columns (n = 3, *** p < 0.001, **** p < 0.0001).

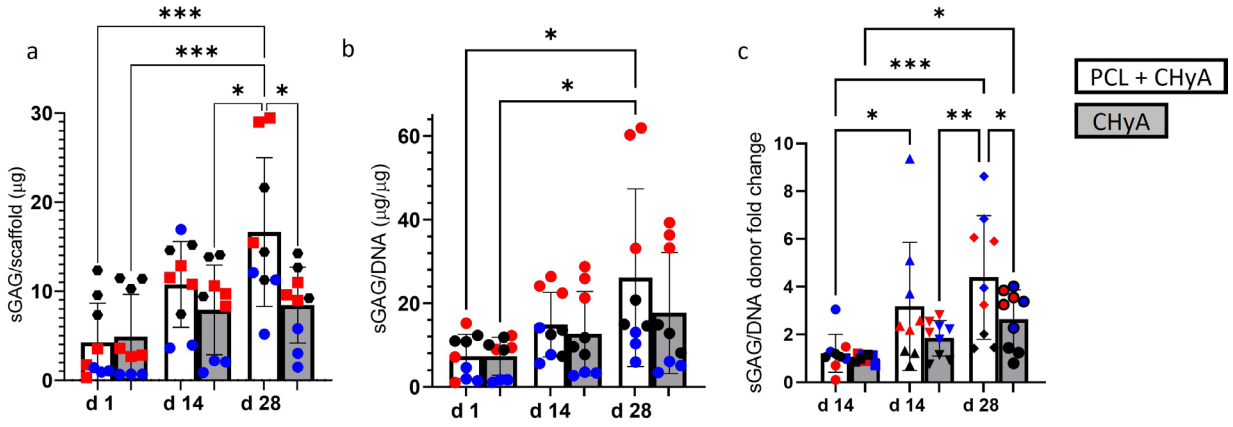

Fig. 5. Cells seeded on PCL-reinforced CHyA scaffold produced more sGAG than CHyA alone. (**a**) Total sGAG deposited by hMSCs seeded on PCL-CHyA (white) or CHyA (grey) after 1, 14 and 28 d incubation in chondrogenic medium (n = 9, * p < 0.05, *** p < 0.001). (**b**) Total sGAG normalised to DNA content per scaffold (n = 9, * p < 0.05). (**c**) sGAG/DNA expressed as a fold change from day 1 CHyA mean values per donor to reduce donor variance in data set (n = 9, * p < 0.05, ** p < 0.01, *** p < 0.001). (**a-c**) Different coloured data points represent biological repeats from different donors.

more centrally located 10 μm sections (Fig. 6 **a**-**h**). Cellular distribution on PCL-CHyA, especially at the central locations, indicated that cells were able to migrate around the PCL struts to reach the centre of a 2 mm-tall PCL-CHyA scaffold (Fig. 6**b**,**d**,**f**,**h**), which was a very satisfactory outcome. Non-reinforced CHyA had similar cellular distribution patterns (Fig. 6**a**,**c**,**e**,**g**) but the cells did not produce sGAG to the same extent as cells on PCL-CHyA scaffolds.

IHC staining for essential articular cartilage structural protein COL2, indicated more cellular deposition on mechanically reinforced PCL-CHyA scaffolds. Representative images of entire cross-sectional slices indicated that hMSCs on both CHyA and PCL-CHyA scaffolds were able to deposit COL2 (Fig. 7 **a**,**b** respectively). Deposition of COL2 on the non-reinforced CHyA matrix was noticeably inferior to the PCL-CHyA sample. Additionally, COL2 was spatially confined to the circumferential perimeter region in the CHyA matrix, whereas the cells within PCL-CHyA scaffold produced a more homogenous spatial distribution of COL2 throughout the cross-sectional area.

Discussion

The objective of the present study was to develop a 3D-printed PCL-reinforced CHyA scaffold with mechanical and biological properties optimised for regeneration of large, load-bearing cartilage defects. Ideally, this bioregenerative platform would be produced as an acellular, off-the-shelf biomaterial capable of secure fixation to the joint surface to facilitate autologous stem cell infiltration, leading to cell-mediated tissue repair. To this end, several different design options were evaluated on application criteria specific for resurfacing large-area defects in articular cartilage. Through this process, two load-bearing scaffold designs, a rectilinear and a gyroid scaffold, were selected and successfully integrated within a CHyA microporous matrix. This incorporation effectively increased the compressive modulus of the CHyA matrix to a range that accurately mimicked healthy cartilage (0.5-2.0 MPa) (Kabir *et al.*, 2021). Importantly, the gyroid scaffold required significantly less force to bend it to the representative curvature of subchondral bone compared to the rectilinear scaffold. All three suture fixation options could withstand more tensile force than was required to bend the gyroid scaffold but only the Twinfix-Ti 2.8 mm osteo-suture anchor was strong enough to bend a rectilinear scaffold effectively to the curvature of condyles. Based on these properties, the gyroid scaffold was the only scaffold brought forward for *in vitro* biological assessment. *In vitro* analysis determined that the reinforced PCL-CHyA scaffold was not inhibiting cellular migration or chondrogenic differentiation of infiltrating MSCs. In fact, the data suggested that the reinforced PCL-CHyA was promoting chondrogenic differentiation more evenly throughout the entire scaffold matrix. The combination of CHyA with the gyroid PCL scaffold provided load-bearing support and secure attachment points to the subchondral bone, all while increasing the chondro-inductiveness of CHyA matrices. These findings indicated that this new 3D-printed PCL-reinforced collagen HyA

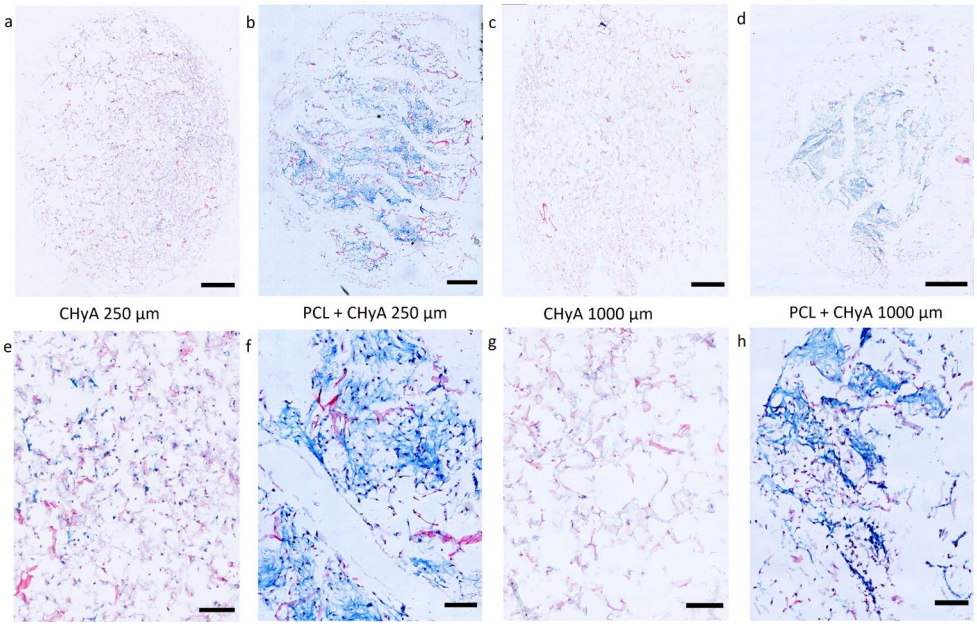

Fig. 6. Histological staining with alcian blue pH 1 and nuclear fast red counterstain confirmed moe cellular sGAG deposition on PCL-CHyA over CHyA after 28 d. (**a**-**d**) Representative mosaic images created by stitching multiple 10× images together to show a complete layer slice of CHyA or PCL-CHyA scaffolds (scale = 1,000 μm). (**a**,**b**,**e**,**f**) Histological slices 250 μm into the respective scaffolds. (**c**,**d**,**g**,**h**) Histological slices from the centre of the 2 mm tall CHyA and PCL-CHyA scaffolds (depth~ 1,000 μm) (**e**-**h** scale bar = 200 μm).

scaffold may have great potential to heal large articular cartilage defects.

Reinforced PCL-CHyA scaffolds retained a homogenous microporous architecture, in line with previous reports of CHyA (Intini *et al*, 2022b; Matsiko *et al*, 2012). Initial concerns that PCL would behave as a thermal insulator or its hydrophobicity would prevent the infiltration of an aqueous ECM and subsequent microporous architecture formation during the freeze-drying process were dismissed after histological and SEM examination of composite PCL-CHyA scaffolds. Surface-treatment of PCL to increase its hydrophilicity with NaOH prior to CHyA infiltration ensured that there was uniform distribution of CHyA throughout the PCL matrix (Visser *et al.*, 2015). Further, analysis of the mean CHyA pore size between CHyA and PCL-CHyA indicated that PCL was not interfering with the formation of the CHyA's microporous architecture (Steele *et al.*, 2022). Successful integration between the PCL scaffold and CHyA matrix represents a merger of materials that offers tuneable mechanical properties, with biomimetic cues that are optimised to support *de novo* hyaline tissue formation (Hutmacher *et al.*, 2001; Martin *et al.*, 2021; Mihajlovic *et al.*, 2022). Alternatively, the methods described in the present study could be adapted and conceivably be transferable to similar load-bearing regenerative medicine applications, such as weight-bearing bone graphs or tooth regeneration with periodontal stem cells (Chang *et al.*, 2020; Lee *et al.*, 2014).

Homogeneous incorporation of CHyA matrix within rectilinear and gyroid design PCL scaffolds increased the compressive modulus by 3 orders of magnitude, effectively mimicking the native properties of hyaline cartilage, overcoming a key limitation of a non-reinforced CHyA matrix (Intini *et al.*, 2022a). The combination of PCL and CHyA did not synergistically increase the compressive modulus as has been reported when IPNs are reinforced with thin fibres of PCL through a MEW process (Schipani *et al.*, 2020; Visser *et al.*, 2015). Visser *et al.* (2015) described how unconfined compression causes individual fibres of a MEW + IPN scaffold to deform, removing the axial porosity and creating a network of confined vertical tubular compartments, resulting in a synergistic increase in compressive modulus. In the present study, the gyroid design, as a result of its variable sinusoidal function, did not align directly above the lower/supporting toolpaths, thus maintaining an interconnected architecture even under deformation (Melchels *et al.*, 2010). As cellular mobility through a PCL-CHyA scaffold was always a concern, as described by Alhadlaq *et al.* (2005), where pre-seeded cells on 3D scaffolds tend to localise near the outer surface of the scaffold, the gyroid design's inherent ability to maintain axial porosity when experiencing load-bearing forces was advantageous to cellular migration in the present study application.

Unlike biomaterials designed for osteochondral defects, which can effectively be press-fitted within the subchondral bone, bioregenerative materials confined to cartilaginous defects present an increased challenge in terms of material fixation, as the adjacent cartilage tissue is not sufficient to support press-fit fixation. A systematic review of cartilage tissue engineering by Patel *et al.* (2019) reported only 3 studies out of 197 tested biomaterial "integration", even though the FDA suggests fixation and integration assessments be performed on biomaterials for cartilage repair in their industry guidance (Web ref. 2). While it is common for engineered cartilage tissue constructs to be assessed for their compressive modulus, less often reported, and a strength of this study, was the investigation of compatible fixation of biomimetic ECM constructs within a large load-bearing cartilage defect (Marchiori *et al.*, 2019). A comparison of chondral biomaterial fixation techniques in large-animal models by Lotz *et al.* (2021) found that many hydrogels show promise *in vitro* but fail *in vivo* due to inadequate fixation within a chondral defect. These data further justify the importance of incorporating a viable fixation strategy early in articular-cartilage biomaterial development. The present study designed the PCL-CHyA bioregenerative scaffolds to be flexible so that they could contour to the curvature of a femoral condyle. Therefore, a suture anchor must be strong enough to overcome the force required to hold PCL scaffolds in a flexed/bent state. Flexibility in a PCL-CHyA scaffold is expected to make it

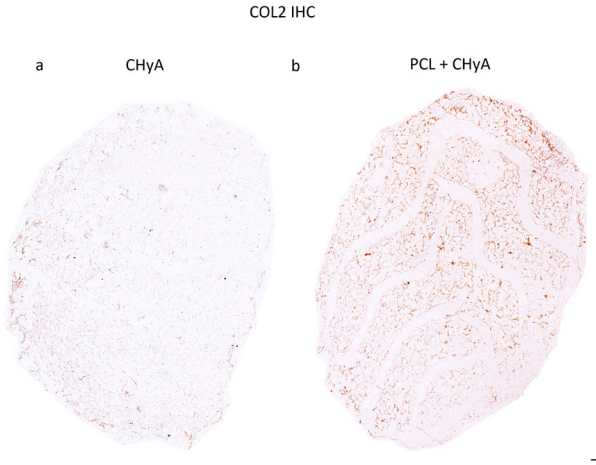

Fig. 7. Larger COL2 deposition from hMSCs on PCL-CHyA scaffolds compared with CHyA. COL2 immunohistochemical staining (1:100, SC-52658) on (**a**) CHyA and (**b**) PCL-CHyA scaffolds after 28 d in culture (scale bar = 1 mm).

easier for a surgeon to manipulate the scaffold, in addition to increasing the compatible fixation options within a chondral defect. Osteo-suture anchors were selected as the preferred fixation method, in agreement with Friedman *et al.* (2018), who found osteo-suture anchors were the best fixation technique in chondral defects when compared with fibrin glue, press-fit fixation or superficial sutures in large-animal weight-bearing models. While the custom 3D-printed subchondral anchors demonstrated varying ability to withstand tensile stress, the commercially available Twinfix Ti's ability to withstand a pull-out force was significantly greater and, as such, was determined as the most appropriate fixation option. The gyroid PCL-CHyA scaffold required 2.6 N of force to bend it but will fail at 22.57 N of tensile force. Therefore, the PLC-CHyA scaffold should be sutured to the subchondral anchor within the tensile range of 2.6-22.57 N to properly fix the scaffold to the subchondral bone. While the Twinfix Ti clearly showed promise, other commercially available bioabsorbable osteo-suture anchors not tested in the present study could conceivably present an attractive alternative to metal osteo-suture anchors (Pill *et al.*, 2021). This knowledge on fixation could contribute to the progression of reinforced biomaterials from the lab through pre-clinical and clinical trials.

Biological evaluation of the reinforced gyroid design PCL-CHyA matrix indicated reinforcement of CHyA with PCL increased cellular sGAG production without negatively affecting cellular migration through the matrix (Fig. 5,6). A similar outcome has been observed by researchers using polymer-reinforced hydrogels for similar cartilage-regenerating applications. Critchley *et al.* (2020) found more sGAG deposition in PCL and PLA reinforced alginate/agarose hydrogels compared to their non-reinforced control. Similarly, Hauptstein *et al.* (2020) also found that reinforcing a HA hydrogel with PCL also leads to increased sGAG deposition when compared with non-reinforced HyA after 21 d in culture. The similarities between these two studies and the experiments described here, with PCL-reinforced ECM mimetic biomaterials resulting in more sGAG deposition compared with their non-reinforced controls, suggests cell mechano-signalling may have a role in the observed phenotypes rather than a material specific response (Bougault *et al.*, 2012; Critchley *et al.*, 2020; Hauptstein *et al.*, 2020; Hecht *et al.*, 2019). Haudenschild *et al.* (2010) reported a direct relationship between the known mechano-sensitive pathway ROCK and the chondrogenic regulator SOX9. ROCK activation results in phosphorylation of SOX9 at serine 181, driving nuclear import of phosphorylated SOX9 (Malki *et al.*, 2005) and allowing SOX9 to act as an essential transcriptional regulator of chondrogenic differentiation. It is possible that PCL reinforcement of scaffolds prevents cell-mediated matrix contraction, resulting in generation of higher tensional forces in the actin cytoskeleton of cells. Conversely, cells in softer, unreinforced scaffolds can "pull" and remodel their microenvironment with less resistance, resulting in correspondingly lower cytoskeleton tension (Ledo *et al.*, 2020). Such a restriction on cell-mediated contraction of scaffolds could also have a significant impact on maintaining CHyA surface area available for cellular attachment or nutrient diffusion through the matrix.

Similar to sGAG findings, IHC analysis indicated higher COL2 protein expression on PCL-CHyA scaffolds compared to non-reinforced CHyA matrices. Besides the level of COL2 production, the differences in spatial distribution, with COL2 deposition being localised near the perimeter of the non-reinforced CHyA matrix, compared with the more homogenous distribution on the PCL-CHyA scaffold was an interesting finding. Although, one section layer represents only a fraction of the total volume of the 3D matrix. While further research would be required to elucidate the specific cellular mechanisms responsible for the effects observed here, these data highlighted the chondrogenic capacity of the PCL-CHyA matrices, a critical indicator of their potential *in vivo* success.

From a translational research perspective, when comparing the freeze-dried PCL-CHyA microporous matrix developed in the present study with PCL-reinforced hydrogels, as described in the previous paragraph (Critchley *et al.*, 2020; Hauptstein *et al.*, 2020), there are distinct attributes that make the freeze-dried scaffolds more attractive than cell-laden PCL-reinforced hydrogels. Firstly, from a logistical perspective, it is easier to store a sterile, dry PCL-CHyA scaffold (Hester *et al.*, 2021). Whereas cell-laden PCL-hydrogels are patient specific, which prevents effective manufacturing at scale since every scaffold made would require donor-specific cells at the time of manufacturing. Then, those patient-specific hydrogels would need constant monitoring to ensure they were stored under culture conditions, with ample nutrient and cytotoxic waste exchange. By comparison, PCL-CHyA matrices when paired with the common surgical technique of microfracture offers a potentially valuable clinical approach, which would release the patient's own bone-marrow-derived MSCs (Guo *et al.*, 2018; Pipino *et al.*, 2019) from the subchondral bone marrow. This is desirable from a translatable research perspective and could be utilised with the scaffold developed in the present study, as it would overcome the need for *ex vivo* manipulation of patient cells, again reducing cost and barriers to translation (Oberweis *et al.*, 2020).

Conclusion

This study has developed a novel reinforced PCL-CHyA scaffold, which might be used to repair large-area articular cartilage defects that currently lack effective treatment options. Utilising 3D printing in the design and biofabrication process allowed mechanical reinforcement to a level similar to

native cartilage of a biomimetic CHyA matrix with bioabsorbable PCL, which also had the benefit of increasing the chondroinductive potential of the CHyA matrix in addition to expanding the size of defects CHyA could effectively treat. Furthermore, the PCL-CHyA scaffold was shown to be compatible with suture fixation to the subchondral bone, addressing the persistent challenge of fixation in the field of bioactive materials for articular cartilage repair. Taken together, this reinforced bioregenerative matrix has significant potential as an off-the-shelf solution for the treatment of large-area chondral defects.

Acknowledgements

This study has received funding from the European Research Council under the European Community's Horizon 2020 research and innovation programme under ERC Advanced Grant agreement number 788753 (ReCaP).

M.J. was responsible for methodology, experimental design, biofabrication, mechanical evaluation, biological evaluation, data processing and manuscript revisions. T.H. contributed to methodology, biological evaluation and manuscript revision. M.L. assisted in methodology and mechanical testing. A.G.V. contributed to conceptualisation, and manuscript revision. D.J.K. was responsible for conceptualisation and manuscript revision. F.J.O. contributed to conceptualisation, funding acquisition, experimental design, methodology and manuscript revision.

References

Alford JW, Cole BJ (2005) Cartilage restoration, part 1: basic science, historical perspective, patient evaluation, and treatment options. Am J Sports Med **33**: 295-306. DOI: 10.1177/0363546504273510.

Alhadlaq A, Mao JJ (2005) Tissue-engineered osteochondral constructs in the shape of an articular condyle. J Bone Jt Surg **87**: 936-944. DOI: 10.2106/JBJS.D.02104.

Barreto S, Gonzalez-Vazquez A, Cameron AR, Cavanagh B, Murray DJ, O'Brien FJ (2017) Identification of the mechanisms by which age alters the mechanosensitivity of mesenchymal stromal cells on substrates of differing stiffness: implications for osteogenesis and angiogenesis. Acta Biomater **53**: 59-69. DOI: 10.1016/j.actbio.2017.02.031.

Bougault C, Aubert-Foucher E, Paumier A, Perrier-Groult E, Huot L, Hot D, Duterque-Coquillaud M, Mallein-Gerin F (2012) Dynamic compression of chondrocyte-agarose constructs reveals new candidate mechanosensitive genes. PLoS One **7**: e36964. DOI: 10.1371/journal.pone.0036964.

Camarero-Espinosa S, Rothen-Rutishauser B, Foster EJ, Weder C (2016) Articular cartilage: from formation to tissue engineering. Biomaterials Science **4**: 734-767. DOI: 10.1039/c6bm00068a.

Chang CC, Lin TA, Wu SY, Lin CP, Chang HH (2020) Regeneration of tooth with allogenous, autoclaved treated dentin matrix with dental pulpal stem cells: an *in vivo* study. J Endod **46**: 1256-1264. DOI: 10.1016/j.joen.2020.05.016.

Chang SH, Lee HJ, Park S, Kim Y, Jeong B (2018) Fast degradable polycaprolactone for drug delivery. Biomacromolecules **19**: 2302-2307. DOI: 10.1021/acs.biomac.8b00266.

Critchley S, Sheehy EJ, Cunniffe G, Diaz-payno P, Carroll SF, Jeon O, Alsberg E, Brama PAJ, Kelly DJ (2020) 3D printing of fibre-reinforced cartilaginous templates for the regeneration of osteochondral defects. Acta Biomater **113**: 130-143. DOI: 10.1016/j.actbio.2020.05.040.

Di Luca A, Van Blitterswijk C, Moroni L (2015) The osteochondral interface as a gradient tissue: from development to the fabrication of gradient scaffolds for regenerative medicine. Birth Defects Res Part C - Embryo Today Rev **105**: 34-52. DOI: 10.1002/bdrc.21092.

DuRaine GD, Arzi B, Lee JK, Lee CA, Responte DJ, Hu JC, Athanasiou KA (2015) Biomechanical evaluation of suture-holding properties of native and tissue-engineered articular cartilage. Biomech Model Mechanobiol **14**: 73-81. DOI: 10.1007/s10237-014-0589-1.

Estes BT, Enomoto M, Moutos FT, Carson MA, Toth JM, Eggert P, Stallrich J, Willard VP, Veis DJ, Little D, Guilak F, Lascelles BDX (2021) Biological resurfacing in a canine model of hip osteoarthritis. Sci Adv **7**: eabi5918. DOI: 10.1126/sciadv.abi5918.

Friedman JM, Sennett ML, Bonadio MB, Orji KO, Neuwirth AL, Keah N, Carey JL, Moutos FT, Estes BT, Guilak F, Madry H, Mauck RL, Dodge GR (2018) Comparison of fixation techniques of 3d-woven poly(ϵ-caprolactone) scaffolds for cartilage repair in a weightbearing porcine large animal model. Cartilage **9**: 428-437. DOI: 10.1177/1947603517700953.

Green BJ, Worthington KS, Thompson JR, Bunn SJ, Rethwisch M, Kaalberg EE, Jiao C, Wiley LA, Mullins RF, Stone EM, Sohn EH, Tucker BA, Guymon CA (2018) Effect of molecular weight and functionality on acrylated poly(caprolactone) for stereolithography and biomedical applications. Biomacromolecules **19**: 3682-3692. DOI: 10.1021/acs.biomac.8b00784.

Guo T, Noshin M, Baker HB, Taskoy E, Meredith SJ, Tang Q, Ringel JP, Lerman MJ, Chen Y, Packer JD, Fisher JP (2018) 3D printed biofunctionalized scaffolds for microfracture repair of cartilage defects. Biomaterials **185**: 219-231. DOI: 10.1016/j.biomaterials.2018.09.022.

Gupta D, Singh AK, Kar N, Dravid A, Bellare J (2019) Modelling and optimization of NaOH-etched 3-D printed PCL for enhanced cellular attachment and growth with minimal loss of mechanical strength. Mater Sci Eng C **98**: 602-611. DOI: 10.1016/j.msec.2018.12.084.

Gupta P, Krishnamoorthy B, Dreifus G (2020) Continuous toolpath planning in a graphical framework for sparse infill additive manufacturing. CAD Comput Aided Des **127**: 1-31. DOI: 10.1016/j.cad.2020.102880.

Haudenschild DR, Chen J, Pang N, Lotz MK, D'Lima DD (2010) Rho kinase-dependent activation of SOX9 in chondrocytes. Arthritis Rheum **62**: 191-200. DOI: 10.1002/art.25051.

Haugh MG, Murphy CM, McKiernan RC, Altenbuchner C, O'Brien FJ (2011) Crosslinking and mechanical properties significantly influence cell attachment, proliferation, and migration within collagen glycosaminoglycan scaffolds. Tissue Eng - Part A **17**: 1201-1208. DOI: 10.1089/ten.tea.2010.0590.

Haugh MG, Murphy CM, O'Brien FJ (2009) Novel freeze-drying methods to produce a range of collagen-glycosaminoglycan scaffolds with tailored mean pore sizes. Tissue Eng Part C Methods **16**: 887-894. DOI: 10.1089/ten.tec.2009.0422.

Hauptstein J, Böck T, Bartolf-Kopp M, Forster L, Stahlhut P, Nadernezhad A, Blahetek G, Zernecke-Madsen A, Detsch R, Jüngst T, Groll J, Teßmar J, Blunk T (2020) Hyaluronic acid-based bioink composition enabling 3D bioprinting and improving quality of deposited cartilaginous extracellular matrix. Adv Healthc Mater **9**: 2000737. DOI: 10.1002/adhm.202000737.

Hecht N, Johnstone B, Angele P, Walker T, Richter W (2019) Mechanosensitive MiRs regulated by anabolic and catabolic loading of human cartilage. Osteoarthr Cartil **27**: 1208-1218. DOI: 10.1016/j.joca.2019.04.010.

Heras Murcia D, Genedy M, Reda Taha MM (2020) Examining the significance of infill printing pattern on the anisotropy of 3D printed concrete. Constr Build Mater **262**: 120559. DOI: 10.1016/j.conbuildmat.2020.120559.

Hester S, Ferenz KB, Eitner S, Langer K (2021) Development of a lyophilization process for long-term storage of albumin-based perfluorodecalin-filled artificial oxygen carriers. Pharmaceutics **13**: 584. DOI: 10.3390/pharmaceutics13040584.

Hodgkinson T, Amado IN, O'Brien FJ, Kennedy OD (2022a) The role of mechanobiology in bone and cartilage model systems in characterizing initiation and progression of osteoarthritis. APL Bioeng **6**: 011501. DOI: 10.1063/5.0068277.

Hodgkinson T, Kelly DC, Curtin CM, O'Brien FJ (2022b) Mechanosignalling in cartilage: an emerging target for the treatment of osteoarthritis. Nat Rev Rheumatol **18**: 67-84. DOI: 10.1038/s41584-021-00724-w.

Hunziker EB, Stähli A (2008) Surgical suturing of articular cartilage induces osteoarthritis-like changes. Osteoarthr Cartil **16**: 1067-1073. DOI: 10.1016/j.joca.2008.01.009.

Hutmacher DW, Schantz T, Zein I, Ng KW, Teoh SH, Tan KC (2001) Mechanical properties and cell cultural response of polycaprolactone scaffolds designed and fabricated *via* fused deposition modeling. J Biomed Mater Res **55**: 203-216. DOI: 10.1002/1097-4636(200105)55:2<203::AID-JBM1007>3.0.CO;2-7.

Intini C, Hodgkinson T, Casey SM, Gleeson JP, O'Brien FJ (2022a) Highly porous type II collagen-containing scaffolds for enhanced cartilage repair with reduced hypertrophic cartilage formation. Bioengineering (Basel) **9**: 232. DOI: 10.3390/bioengineering9060232.

Intini C, Lemoine M, Hodgkinson T, Casey S, Gleeson JP, O'Brien FJ (2022b) A highly porous type II collagen containing scaffold for the treatment of cartilage defects enhances MSC chondrogenesis and early cartilaginous matrix deposition. Biomater Sci **10**: 970-983. DOI: 10.1039/d1bm01417j.

Kabir W, Di Bella C, Choong PFM, O'Connell CD (2021) Assessment of native human articular cartilage: a biomechanical protocol. Cartilage **13**: 427S-437S. DOI: 10.1177/1947603520973240.

Layton C, Bancroft JD (2019) Carbohydrates. In: Bancroft's theory and practice of histological techniques. Elsevier. pp: 176-197. DOI: 10.1016/B978-0-7020-6864-5.00013-X.

Ledo AM, Vining KH, Alonso MJ, Garcia-Fuentes M, Mooney DJ (2020) Extracellular matrix mechanics regulate transfection and SOX9-directed differentiation of mesenchymal stem cells. Acta Biomater **110**: 153-163. DOI: 10.1016/j.actbio.2020.04.027.

Lee CH, Hajibandeh J, Suzuki T, Fan A, Shang P, Mao JJ (2014) Three-dimensional printed multiphase scaffolds for regeneration of periodontium complex. Tissue Eng - Part A **20**: 1342-1351. DOI: 10.1089/ten.tea.2013.0386.

Levingstone TJ, Moran C, Almeida HV, Kelly DJ, O'Brien FJ (2021) Layer-specific stem cell differentiation in tri-layered tissue engineering biomaterials: towards development of a single-stage cell-based approach for osteochondral defect repair. Mater Today Bio **12**: 100173. DOI: 10.1016/j.mtbio.2021.100173.

Levingstone TJ, Ramesh A, Brady RT, Brama PAJ, Kearney C, Gleeson JP, O'Brien FJ (2016) Cell-free multi-layered collagen-based scaffolds demonstrate layer specific regeneration of functional osteochondral tissue in caprine joints. Biomaterials **87**: 69-81. DOI: 10.1016/j.biomaterials.2016.02.006.

Levingstone TJ, Sheehy EJ, Moran CJ, Cunniffe GM, Diaz Payno PJ, Brady RT, Almeida HV, Carroll SF, O'Byrne JM, Kelly DJ, Brama PA, O' Brien FJ (2022) Evaluation of a co-culture of rapidly isolated chondrocytes and stem cells seeded on tri-layered collagen-based scaffolds in a caprine osteochondral defect model. Biomater Biosyst **8**: 100066. DOI: 10.1016/j.bbiosy.2022.100066.

Liu H, Ahlinder A, Yassin MA, Finne-Wistrand A, Gasser TC (2020) Computational and experimental characterization of 3D-printed PCL structures toward the design of soft biological tissue scaffolds. Mater Des **188**: 108488. DOI: 10.1016/j.matdes.2020.108488.

Lotz B, Bothe F, Deubel A-K, Hesse E, Renz Y, Werner C, Schäfer S, Böck T, Groll J, von Rechenberg B, Richter W, Hagmann S (2021) Preclinical testing of new hydrogel materials for cartilage repair: overcoming fixation issues in a large animal model. Int J Biomater **2021**: 1-14. DOI: 10.1155/2021/5583815.

MacCraith E, Joyce M, do Amaral RJFC, O'Brien FJ, Davis NF (2022) Development and *in vitro* investigation of a biodegradable mesh for the treatment of stress urinary incontinence. Int Urogynecol J **33**: 2177-2184. DOI: 10.1007/s00192-022-05160-2.

Malki S, Nef S, Notarnicola C, Thevenet L, Gasca S, Méjean C, Berta P, Poulat F, Boizet-Bonhoure B (2005) Prostaglandin D2 induces nuclear import of the sex-determining factor SOX9 *via* its cAMP-PKA phosphorylation. EMBO J **24**: 1798-1809. DOI: 10.1038/sj.emboj.7600660.

Marchiori G, Berni M, Boi M, Filardo G (2019) Cartilage mechanical tests: evolution of current standards for cartilage repair and tissue engineering. A literature review. Clin Biomech **68**: 58-72. DOI: 10.1016/j.clinbiomech.2019.05.019.

Martin AR, Patel JM, Locke RC, Eby MR, Saleh KS, Davidson MD, Sennett ML, Zlotnick HM, Chang AH, Carey JL, Burdick JA, Mauck RL (2021) Nanofibrous hyaluronic acid scaffolds delivering TGF-β3 and SDF-1α for articular cartilage repair in a large animal model. Acta Biomater **126**: 170-182. DOI: 10.1016/j.actbio.2021.03.013.

Matsiko A, Gleeson JP, O'Brien FJ (2014) Scaffold mean pore size influences mesenchymal stem cell chondrogenic differentiation and matrix deposition. Tissue Eng Part A **21**: 486-497. DOI: 10.1089/ten.tea.2013.0545.

Matsiko A, Levingstone TJ, Gleeson JP, O'Brien FJ (2015) Incorporation of TGF-beta 3 within collagen-hyaluronic acid scaffolds improves their chondrogenic potential. Adv Healthc Mater **4**: 1175-1179. DOI: 10.1002/adhm.201500053.

Matsiko A, Levingstone TJ, O'Brien FJ, Gleeson JP (2012) Addition of hyaluronic acid improves cellular infiltration and promotes early-stage chondrogenesis in a collagen-based scaffold for cartilage tissue engineering. J Mech Behav Biomed Mater **11**: 41-52. DOI: 10.1016/j.jmbbm.2011.11.012.

Melchels FPW, Bertoldi K, Gabbrielli R, Velders AH, Feijen J, Grijpma DW (2010) Mathematically defined tissue engineering scaffold architectures prepared by stereolithography. Biomaterials **31**: 6909-6916. DOI: 10.1016/j.biomaterials.2010.05.068.

Mihajlovic M, Rikkers M, Mihajlovic M, Viola M, Schuiringa G, Ilochonwu BC, Masereeuw R, Vonk L, Malda J, Ito K, Vermonden T (2022) Viscoelastic chondroitin sulfate and hyaluronic acid double-network hydrogels with reversible cross-links. biomacromolecules. DOI: 10.1021/acs.biomac.1c01583.

Moers-Carpi MM, Sherwood S (2013) Polycaprolactone for the correction of nasolabial folds: a 24-month, prospective, randomized, controlled clinical trial. Dermatologic Surg **39**: 457-463. DOI: 10.1111/dsu.12054.

Nehrer S, Breinan HA, Ramappa A, Hsu HP, Minas T, Shortkroff S, Sledge CB, Yannas IV, Spector M (1998) Chondrocyte-seeded collagen matrices implanted in a chondral defect in a canine model. Biomaterials **19**: 2313-2328. DOI: 10.1016/S0142-9612(98)00143-4.

Nieminen MT, Töyräs J, Laasanen MS, Silvennoinen J, Helminen HJ, Jurvelin JS (2004) Prediction of biomechanical properties of articular cartilage with quantitative magnetic resonance imaging. J Biomech **37**: 321-328. DOI: 10.1016/S0021-9290(03)00291-4.

Oberweis CV, Marchal JA, López-Ruiz E, Gálvez-Martín P (2020) A worldwide overview of regulatory frameworks for tissue-based products. Tissue Eng - Part B Rev **26**: 181-196. DOI: 10.1089/ten.teb.2019.0315.

Patel JM, Wise BC, Bonnevie ED, Mauck RL (2019) A systematic review and guide to mechanical testing for articular cartilage tissue engineering. Tissue Eng - Part C Methods **25**: 593-608. DOI: 10.1089/ten.tec.2019.0116.

Pill SG, McCallum J, Tolan SJ, Bynarowicz T, Adams KJ, Hutchinson J, Alexander R, Siffri PC, Brooks JM, Tokish JM, Kissenberth MJ (2021) Regenesorb and polylactic acid hydroxyapatite anchors are associated with similar osseous integration and rotator cuff healing at 2 years. J Shoulder Elb Surg **30**: S27-S37. DOI: 10.1016/j.jse.2021.04.003.

Pipino G, Risitano S, Alviano F, WU EJ, Bonsi L, Vaccarisi DC, Indelli PF (2019) Microfractures and hydrogel scaffolds in the treatment of osteochondral knee defects: a clinical and histological evaluation. J Clin Orthop Trauma **10**: 67-75. DOI: 10.1016/j.jcot.2018.03.001.

Schipani R, Scheurer S, Florentin R, Critchley SE, Kelly DJ (2020) Reinforcing interpenetrating network hydrogels with 3D printed polymer networks to engineer cartilage mimetic composites. Biofabrication **12**: 035011. DOI: 10.1088/1758-5090/ab8708.

Stack JD, Levingstone TJ, Lalor W, Sanders R, Kearney C, O'Brien FJ, David F (2017) Repair of large osteochondritis dissecans lesions using a novel multilayered tissue engineered construct in an equine athlete. J Tissue Eng Regen Med **11**: 2785-2795. DOI: 10.1002/term.2173.

Steele JAM, Moore AC, St-Pierre J-P, McCullen SD, Gormley AJ, Horgan CC, Black CR, Meinert C, Klein T, Saifzadeh S, Steck R, Ren J, Woodruff MA, Stevens MM (2022) *In vitro* and *in vivo* investigation of a zonal microstructured scaffold for osteochondral defect repair. Biomaterials **286**: 121548. DOI: 10.1016/j.biomaterials.2022.121548.

Unterman SA, Gibson M, Lee JH, Crist J, Chansakul T, Yang EC, Elisseeff JH (2012) Hyaluronic acid-binding scaffold for articular cartilage repair. Tissue Eng Part A **18**: 2497-2506. DOI: 10.1089/ten.tea.2011.0711.

Visser J, Melchels FPW, Jeon JE, van Bussel EM, Kimpton LS, Byrne HM, Dhert WJA, Dalton PD, Hutmacher DW, Malda J (2015) Reinforcement

of hydrogels using three-dimensionally printed microfibres. Nat Commun **6**: 6933. DOI: 10.1038/ncomms7933.

Zhang P, Arceneaux DJ, Khattab A (2018) Mechanical properties of 3D printed polycaprolactone honeycomb structure. J Appl Polym Sci **135**: 46018. DOI: 10.1002/app.46018.

Web References

1. https://image-ppubs.uspto.gov/dirsearch-public/print/downloadPdf/9215882 [15-06-2023]

2. https://www.fda.gov/regulatory-information/search-fda-guidance-documents/preparation-ides-and-inds-products-intended-repair-or-replace-knee-cartilage [15-06-2023]

Discussion with Reviewers

Reviewer 1: What is the best biomaterial composition for articular cartilage regeneration that shall be transferred to the clinic based on these findings and the experience of the authors?
Authors: This is a somewhat broad question as there are so many different biomaterials with a broad range of compositions that have been utilised and this question is still debated within the research field. However, we do feel that the combination of the PCL with the CHyA is a promising option. When referring specifically to the ratio of collagen type I, COL2 and HyA in CHyA, the present study incorporated the conclusion of Intini *et al.* (2022b), who compared different CHyA matrix compositions and found that equal parts of collagen type I and II with HyA showed the greatest promise for articular cartilage applications.

Reviewer 1: What are the mechanical properties of the regenerated tissues compared to mature hyaline cartilage? Is the engineered tissue integrated with the surrounding cartilage?
Authors: Although it would be interesting to know, not enough samples were availabled to test this. However, it is doubtful that the PCL would have degraded much in 28 d. Therefore, we would expect the compressive modulus to closely resemble that of an acellular PCL-CHyA scaffold, which does fall within the range of healthy articular cartilage's compressive modulus (0.5-2.0 Mpa) in humans. Based on *in vitro* evidence published by Matsiko *et al.* (2012), characterising the change in compressive modulus of non-reinforced ChyA after being seeded with MSCs over 28 d, the additional mechanical properties provided by cell presence and ECM distribution increased CHyA's modulus by ~ 1 KPa, which is orders of magnitude below the PCL-CHyA scaffold's compressive modulus.

Reviewer 2: How can bio-integration at the edges of the defect be envisaged with this type of scaffold, which offers a certain mechanical resistance but does not guarantee bio-integration with the native cartilage?
Authors: This will be explored further with *in vivo* experiments. Initially, cylindrical scaffolds were tested *in vitro*, as they were a simple shape for a surgeon to match when they are debriding the damaged cartilage, with a snug fitting PCL-CHyA scaffold offering the best chance of integration. When planning the toolpath designs of the cylindrical scaffolds, a standard "perimeter" toolpath was removed, to facilitate cells migration laterally, in or out of the scaffold. Implantation of PCL-CHyA is planned to be accompanied by a microfracture surgical technique to provide endogenous hMSCs as it is unlikely that many cells would be migrating laterally through the dense cartilage matrix into PCL-CHyA, although future *in vivo* tests would be needed to determine how well PCL-CHyA integrates with surrounding hyaline tissue. Based on previous research by Levingstone *et al.* (2016) showing cells ability to migrate into a similar non-reinforced microporous scaffold *in vivo*, combined with the present study *in vitro* findings showing that PCL did not severely inhibit cellular migration, we are optimistic in PCL-CHyA's potential to be integrated with the surrounding tissue *in vivo*.

Reviewer 2: In the context of a clinical protocol, how can cell migration to colonise the scaffold and the quality of the cartilage tissue synthesised be guaranteed?
Authors: While *in vivo* studies using the PCL-CHyA scaffolds were not performed, previous research by Levingstone *et al.* (2016) demonstrated that cell-free microporous scaffolds were integrating well in caprine joints 2 weeks after implantation, with impressive cell and tissue integration being quantified after 3 months. Having demonstrated in the present study that hMSCs are able to migrate unassisted through the PCL-CHyA scaffold to its centre, we are optimistic that *in vivo* studies would have similar success. As far as characterising the quality of newly synthesised cartilage in a clinical setting, MRI scans could offer non-invasive imaging to assess the quality of the tissue regenerating in the defected region.

Editor's note: The Scientific Editor responsible for this paper was Martin Stoddart.